Available online at www.eccomasproceedia.org
Eccomas Proceedia COMPDYN (2023) 2554-2565

ECCOMAS
Proceedia

COMPDYN 2023
9th ECCOMAS Thematic Conference on
Computational Methods in Structural Dynamics and Earthquake Engineering
M. Papadrakakis, M. Fragiadakis (eds.)
Athens, Greece, 12-14 June 2023

SAFE DESIGN OF SUBSEA PIPELINES TO COMBINED SEISMIC AND THERMAL LOADING

Daniele Mina[1], Hassan Karampour[1,*], and Davide Forcellini[2]

[1] Griffith University
Southport QLD 4222, Australia
e-mail: d.mina@griffith.edu.au; h.karampour@griffith.edu.au

[2] University of Canterbury
Christchurch, New Zealand
davide.forcellini@canterbury.ac.nz

*: corresponding author

Abstract

The current work uses validated finite element models to evaluate the performance of high pressure-high temperature (HP/HT) offshore pipelines to combined seismic and operational loads. Safety of the pipeline is investigated under different load-paths and with different pipe-soil interaction models. In a parametric study, structural responses of the pipeline SDR (diameter to wall-thickness ratio) at different in-service temperatures are assessed. Results are compared to codified recommendations. It is shown that in offshore pipelines with larger SDR, typically used in shallow waters, the combined loading imposes a higher risk.

Keywords: HP/HT pipelines, Thermal buckling, Local buckling, Earthquake, Combined seismic-thermal loading, Offshore pipeline.

ISSN:2623-3347
Peer-review under responsibility of the organizing committee of COMPDYN 2023.
doi: 10.7712/120123.10582.20913

1 INTRODUCTION

Pipeline resilience to natural and man-made hazards plays a significant role in the design process of these essential infrastructures and has a great impact on both society and the environment [1]. Both offshore and onshore pipelines are prone to failure due to natural and operational loads. Offshore pipelines and risers are employed for transport of hydrocarbons in deeper waters and harsher conditions (for instance, the deepest gas pipeline laid by Shell in the Stones field in the US Gulf of Mexico [2]). In such environments, thicker pipelines with the OD/t ratio as low as 10 are required due to the substantial hydrostatic pressure [3-6]. Moreover, the pipeline may need to be installed on seabed with escarpments that increases the risk of thermal buckling [7–9], free-spanning [10] and vortex-induced vibrations [11]. The interaction between thermal loading and local collapse poses strict design conditions for this type of infrastructures, and has been studied experimentally [7,8] and numerically [12] in rigid pipelines and pipe-in-pipe systems [13,14].

In this scenario, seismic loading must be considered when assessing the resilience of pipelines. Strong evidence of the wave propagation damages inflicted to buried natural gas (NG) pipelines [15–22] suggest that earthquakes can cause long service disruptions, leading to unpredictably high direct and indirect socioeconomic losses in unprepared communities. Many authors proposed models to evaluate the structural performance and repair costs of pipelines subject to ground seismic wave propagation or permanent ground movements [23–28]. American Lifelines Alliance (ALA, [29]) proposed seismic fragility formulations for structural components of WDS, such as pipelines, tanks, and other water supply facilities.

While several studies focus on the seismic response of onshore pipelines [23–32], the behaviour of submerged pipelines under earthquake action is marginally addressed [33,34]. The internationally renowned standard for design of submarine pipelines systems, DNV [35], recommends limit state design of global and local buckling of pipelines under combined bending, axial force, and pressure. However, in seismic design, DNV [35] permits the designer to consider earthquake as an accidental load and suggests conducting a safety check based on the probability of occurrence. The recommended practice for structural analysis of piping systems DNV [36], allows quasi-static or dynamic analysis of pipelines under earthquake actions. In case of quasi-static analysis, a load magnifier known as dynamic load factor (DLF) as large as 1.5-2.0 is mandated [36]. However, dynamic analyses methods such as modal analysis, harmonic analysis, response spectrum analysis and time-history analysis are preferred, and are known to provide more accurate prediction of the seismic-induced stresses in the pipeline. Thus, in the current work a modal analysis is conducted to acquire the modal properties of the pipeline and is followed by a response spectrum analysis to obtain the thermos-seismic interactions, as will be explained in the upcoming sections.

Current authors previously investigated the potential failure of a typical HP/HT pipeline based on fragility analysis and subject to combined seismic and thermal loading [33]. The presented study aims to consider the combined effects of internal pressure, thermal and earthquake loads, to provide some information on design and acceptance criteria for the possible structural failure of subsea pipelines with outside diameter-to-wall thickness ratio (OD/t) between 10 (used in ultra-deep waters) and 50 (used in onshore and/or shallow waters) and to assess their resilience. The following are studied herein and in the following order: (1) prediction of local buckling in the pipelines due to bending; finite element analysis (FEA) and code compliancy, (2) thermal buckling study using FEA and proposing novel empirical design equations, (3) thermo-seismic coupling study including a parametric investigation, and (4) a resilience assessment.

2 LOCAL BUCKLING

2.1 Finite Element Analysis (FEA)

As described by Karampour et al. [8] in a globally buckled pipeline, the local collapse due to combined pressure and thermal buckle is dominated by the bending, and the effects of axial forces are negligible. Accordingly, finite element analyses (FEA) using commercial package ABAQUS [37] were performed in order to investigate the pure bending response of the pipelines with different *OD*/*t* represented in Table 1. For simplicity, the outside diameter (*OD*) is changed while wall thickness t = 12.7 mm is maintained constant. The pipelines are modelled with 4-node doubly curved shell elements (S4R) and 13 thickness integration points using Simpson integration rule [37]. Bilinear stress-strain constitutive material was defined, in order to investigate the effects on the ultimate moment capacity and strains of the pipelines, following experimental results by Binazir et al. [13]. The modelling is explained in detail in a previous work, Mina et al. [33] and is not repeated here again for sake of brevity. Results are shown in Figure 1, where moment M is normalised to the plastic moment M_P of the pipe, and curvature χ is normalised to the critical curvature χ_c. Overall, in all pipelines modelled herein nonlinear bending response is observed at normalised moments $M/M_P > 0.8$, like the experimental observations [38].

$$\boldsymbol{M_P = \sigma_y (D-t)^2 t} \quad ; \quad \boldsymbol{\chi_c = \frac{t}{(D-t)^2}} \tag{1}$$

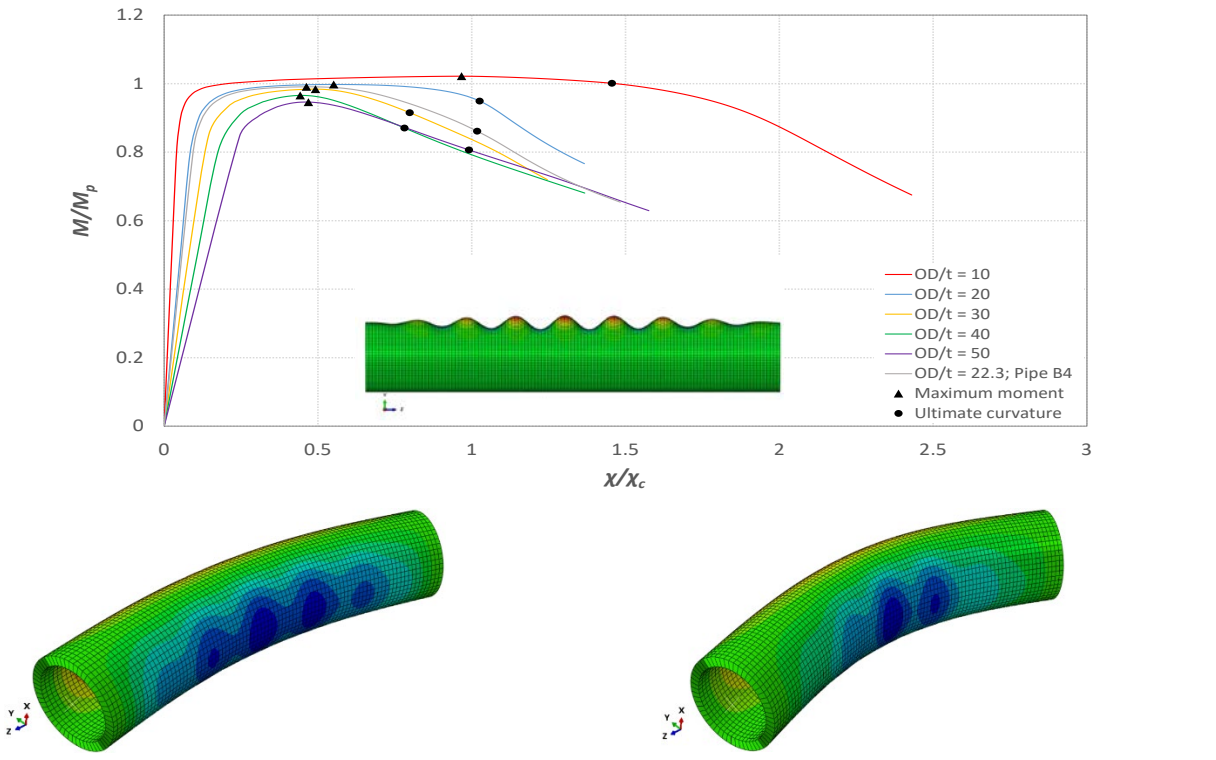

Figure 1: The moment-curvature response of the pipeline with different *OD*/*t* under pure bending and the imposed imperfection shape, and buckled shape at the maximum moment (left) and ultimate curvature (right) of the pipeline with *OD*/*t*=10.

2.2 Local buckling in standards

According to DNV [35], for a pipeline subjected to longitudinal compressive strain induced by bending moment and axial force and internal overpressure (internal pressure in excess of the external hydrostatic pressure), the following design condition should be satisfied at all cross-sections:

$$\boldsymbol{\varepsilon_{Sd} \leq \varepsilon_{Rd} = \frac{\varepsilon_c}{\gamma_\varepsilon}}$$

$$\varepsilon_{\mathrm{c}} = 0.78 \cdot \left(\frac{t}{OD} - 0.01\right) \cdot \left(1 + 5.75 \cdot \frac{p_i - p_e}{p_b}\right) \cdot \alpha_h^{-1.5} \cdot \alpha_{gw}$$

$$\mathrm{p_b} = \frac{2 \cdot \mathrm{t}}{\mathrm{OD} - \mathrm{t}} \cdot \mathrm{f_{cb}} \cdot \frac{2}{\sqrt{3}} \qquad (2)$$

$$f_{cb} = min\left[\sigma_y; \frac{\sigma_u}{1.15}\right]$$

where ε_{Sd} is the design compressive strain, ε_c is the characteristic bending strain resistance, p_i and p_e are the internal and external pressures and p_b is the burst pressure. The strain hardening parameter α_h is equal to 0.93 for C-Mn steel pipe and the girth weld factor α_{gw} is equal to 1. The resistance strain factor γ_ε for 3 different classes, low, medium, and high, are equal to 2.0, 2.5 and 3.3, respectively [35]. Table 1 represents the normalised moment and curvature, and the compressive strains for the considered OD/t, at maximum bending moment and at ultimate curvature, respectively. The strain at maximum bending moment is the critical strain (limit value for local buckling). The internal pressure is assumed to be 12 MPa higher than the external pressure in all pipelines. The ultimate moment capacity is reached at $1.022M_P$, $0.998M_P$, $0.984M_P$, $0.966M_P$ and $0.946M_P$ for OD/t of 10, 20, 30, 40 and 50, respectively. FEA results show that the ultimate strains at Stage I (critical strains) are closer to the low safety class [35] with the increase in OD/t (see Table 1). This is mainly because of higher risk of failure due to local collapse in thinner pipes ($OD/t > 30$). A different trend is followed by the pipe with $OD/t = 10$, characterised by a critical strain which only differs from low class design strain ε_{Sd} by 10.2%. The pipeline with $OD/t = 20$ shows the closest critical strain comparable to the high safety class.

Table 1: Comparison between compressive strains (εc) at maximum moment and at ultimate curvature and the design compressive strains (εSd) of the studied pipelines with an internal pressure of 12 MPa according to DNV [35]

OD/t	P_b (MPa)	ε_c from FEA (mm/mm)		ε_{Sd} (Eq. (2)) for different safety classes (mm/mm)		
		At max. moment (Stage I)	At ultimate curvature (Stage II)	low	medium	high
10	115	6.904×10^{-2}	1.056×10^{-1}	6.263×10^{-2}	5.010×10^{-2}	3.796×10^{-2}
20	55	2.595×10^{-2}	6.614×10^{-2}	3.943×10^{-2}	3.155×10^{-2}	2.390×10^{-2}
30	36	2.359×10^{-2}	3.516×10^{-2}	2.977×10^{-2}	2.382×10^{-2}	1.804×10^{-2}
40	27	2.065×10^{-2}	2.342×10^{-2}	2.349×10^{-2}	1.879×10^{-2}	1.424×10^{-2}
50	21	1.859×10^{-2}	1.974×10^{-2}	1.856×10^{-2}	1.485×10^{-2}	1.125×10^{-2}

3 THERMAL BUCKLING

The lateral buckling of the studied pipelines with geometrical properties represented in Table 1, is analysed herein as shown in Figure 2. The studied pipelines are modelled using 2-node linear pipe elements (PIPE31) [37], and laid on a sleeper connected to a discrete rigid surface.

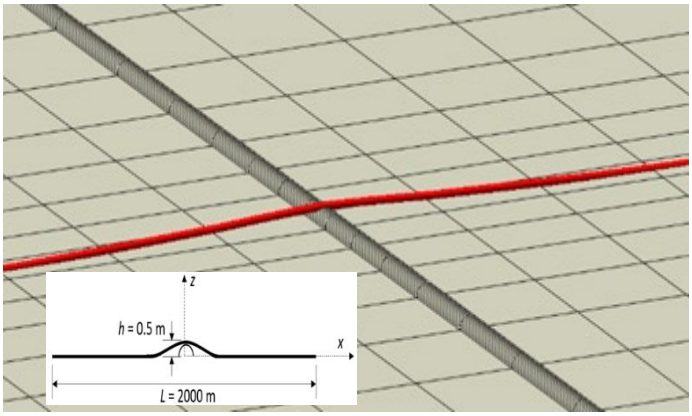

Figure 2: The pipeline/sleeper intersection in the FEA.

The soil-pipeline and the pipeline-sleeper interaction is modelled using Mohr's friction. The pipeline has a length of 2000 m, the sleeper height is equal to 0.5 m, and the seabed and sleeper friction coefficients are 0.5 and 0.3, respectively. Validation of the FEA is given in Mina et al. [33] and is not repeated herein for the sake of brevity. Firstly, the pipeline is subjected to a weight of 1,500 N/m to obtain the initial deformed shape (Figure 2). The analytical formulation is given in Karampour et al. [8]. Then, internal pressure is increased up to 12 MPa. Finally, the temperature of the pipeline is increased until a global instability known as lateral buckling is observed [12]. Figure 3 shows the thermal buckling response of the pipeline from a quasi-static analysis. The temperature is increased up to a critical value, after which the buckle amplitude monotonically upsurges with the corresponding increase in the temperature. The lateral buckle profile at different temperatures is shown in Figure 3 and clearly shows the sudden jump in the crown displacement at the critical temperature. The lateral profiles observed herein (in all *OD*/*t*) are known as Hobbs' third mode [41], which is identified by a distinctive local buckle and two adjacent smaller lobes. As the temperature goes beyond the critical point, the mid-lobe grows at a larger rate compared to the adjacent buckled lobes.

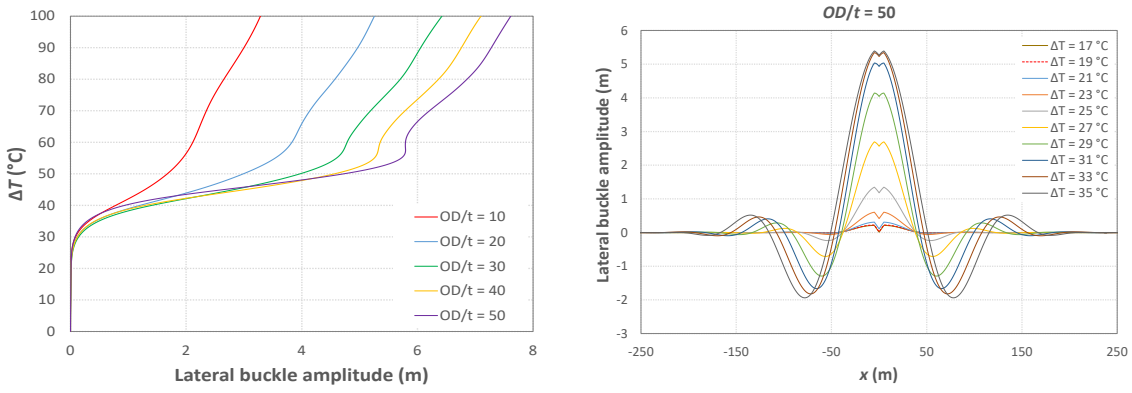

Figure 3: Thermal buckling responses of the pipelines showing temperature vs. crown buckle deformation (left) and buckle profile of the pipeline with *OD*/*t*=50 (right)

Maximum compressive strains at the crown segment of all the studied pipelines are presented in Table 2. Even at temperatures larger than the critical temperature (underlined in Table 2), the compressive strains are smaller than those outlined in Table 1 for low safety class design and are lower than the strains corresponding to the ultimate moment capacity.

Table 2: Maximum values of compressive strain in the buckle crown (ε_c, expressed in mm/mm) for the considered temperature range. Critical temperatures are underlined.

	10	20	30	40	50
OD/t	ε_c (mm/mm)	ε_c (mm/mm)	ε_c (mm/mm)	ε_c (mm/mm)	ε_c (mm/mm)
17	1.767×10^{-3}	1.360×10^{-3}	1.322×10^{-3}	1.045×10^{-3}	9.140×10^{-4}
19	1.802×10^{-3}	1.409×10^{-3}	1.364×10^{-3}	1.080×10^{-3}	$\underline{9.353\times10^{-4}}$
21	1.840×10^{-3}	1.463×10^{-3}	1.404×10^{-3}	$\underline{1.090\times10^{-3}}$	9.317×10^{-4}
23	1.877×10^{-3}	1.517×10^{-3}	$\underline{1.441\times10^{-3}}$	1.047×10^{-3}	9.917×10^{-4}
25	1.913×10^{-3}	$\underline{1.588\times10^{-3}}$	1.437×10^{-3}	1.220×10^{-3}	1.354×10^{-3}
27	$\underline{1.952\times10^{-3}}$	1.714×10^{-3}	1.385×10^{-3}	1.687×10^{-3}	1.852×10^{-3}
29	1.987×10^{-3}	1.955×10^{-3}	1.758×10^{-3}	2.094×10^{-3}	2.200×10^{-3}
31	2.026×10^{-3}	2.066×10^{-3}	2.089×10^{-3}	2.178×10^{-3}	2.236×10^{-3}
33	2.058×10^{-3}	2.063×10^{-3}	2.164×10^{-3}	2.164×10^{-3}	2.267×10^{-3}
35	2.087×10^{-3}	2.046×10^{-3}	2.211×10^{-3}	2.155×10^{-3}	2.300×10^{-3}

4 COMBINED THERMAL-SEISMIC LOADING

Knowing the critical temperatures from previous section, two load-paths are probable: (1) earthquake event after the buckle is initiated, and (2) earthquake event at temperatures lower than the critical temperature. Previous study by current authors [33] showed that the first load path is more critical. Therefore, in the current study, load path (1) is chosen to investigate the thermal-seismic performance of the pipelines. Since the pipeline is characterized by a composite material (steel pipeline with concrete coating), a damping ratio of 3% is chosen, as proposed by Kalliontzis [48] and DNV [49], and is applied to the pipeline material properties in the form of Rayleigh damping coefficients. In the current study, the most detrimental earthquake input motion of the total 17 previously analysed by Mina et al. [33] (Northridge 1994, [50]) is taken into account, and the dynamic response of the pipeline with different *OD*/*t* ratios is analysed. Time histories of the midpoint maximum compressive strain and the lateral buckle amplitude at various stages of the loading and for all the considered pipelines are displayed in Figure 4.

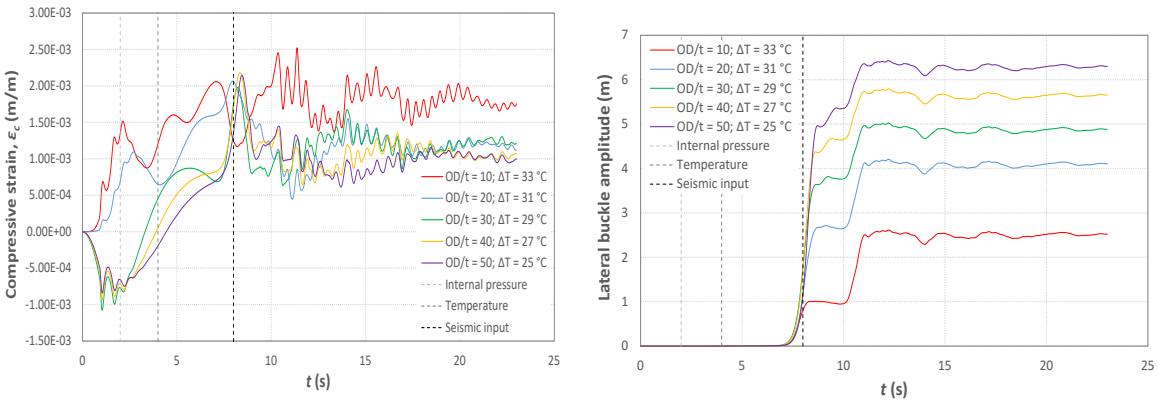

Figure 4: Thermal-seismic interaction results in terms of (a) maximum compressive strain ε_c, (b) and lateral displacement time histories of the buckle crown.

Lateral displacement is larger for high values of OD/t. The highest jump in buckle amplitude is in the pipeline with OD/t of 10 (from 1 m to 2.5 m), as shown in Figure 4. The risk of failure due to excessive curvature in the pipeline is assessed by comparing the lateral buckle curvature, χ_{LB} calculated from Eq. (6), to the curvature at maximum moment capacity, χ_I calculated from the FEA bending results in the first section of this article. Assuming sinusoidal expressions for the lateral buckle lobes, it is straightforward to show that the lateral buckle curvature χ_{LB} in the crown is equal to [12]:

$$\boldsymbol{\chi_{LB} = \frac{\pi^2 \Delta_{LB}}{L_{LB}^2}} \tag{1}$$

where Δ_{LB} and L_{LB} are the buckle amplitude and buckle half-wave lengths, respectively. The curvatures at post-seismic response of the laterally buckled pipes are represented in Table 3. The curvature at maximum moment, Stage I, of flexural response of the pipelines. The safety factor (SF) is defined as the inverse of the ratio R of the crown curvature of the pipeline to its curvature at Stage I χ_I of bending response of the corresponding pipeline. A safety factor smaller than 1 is interpreted as failure due to local buckling (wrinkling in compression) of the pipeline. It can be seen that SF is higher for low OD/t values, meaning that for thicker pipelines the thermal-seismic interaction has a little-to-no effect on the local buckling. Pipelines with $OD/t >$ 40 are more vulnerable to local buckling failure in combined thermal and seismic actions. The lowest safety factor is registered for OD/t = 50, which is equal to 0.88, highlighting the high risk of failure due to the combined loading in pipeline used in shallow waters.

Table 3: Safety factors corresponding to thermal-seismic interaction.

OD/t	χ_I (Figure 1)	χ_{LB} (Eq. (6))	$R = \chi_{LB}/\chi_I$	$SF = 1/R$
10	0.9402	6.440×10^{-2}	6.849×10^{-2}	14.60
20	0.1202	3.586×10^{-2}	2.982×10^{-1}	3.35
30	0.0461	2.415×10^{-2}	5.245×10^{-1}	1.91
40	0.0229	1.892×10^{-2}	8.259×10^{-1}	1.21
50	0.0154	1.755×10^{-2}	1.140	0.88

5 VARIATION OF SEABED-PIPE FRICTION AND SUBMERGED WEIGHT

In this section, the effects of pipe-seabed-sleeper friction and submerged weight variation on a pipeline with OD/t = 20 are investigated. In this regard, different analyses are conducted: firstly, seabed-pipe friction coefficient μ_1 is increased from 0.3 to 0.9; then, the sleeper-pipe friction coefficient μ_2 varies from 0.1 to 0.7; finally, the combined effect of pipe-seabed-sleeper friction coefficients is analysed. The submerged weight q, which corresponds to the first loading step, is increased from 1000 N/m to 3000 N/m. The control sample has q = 1500 N/m, μ_1 = 0.5 and μ_2 = 0.3. The temperature is kept at 31 °C (critical temperature, as described in [33]). Table 4 reports maximum values in pre- and post-earthquake loading.

When both friction coefficients μ_1 and μ_2 increase, the maximum buckle displacement in the pipeline midpoint decreases from 4.32 m to 2.78 m. With only μ_2 reduced to 0.1, the buckle crown displacement grows up to 4.38 m. The same trend, characterised by larger lateral displacement for low values of q, is registered when the submerged weight varies, and the absolute

lateral displacement becomes significantly lower by rising q value, and the reduction is 76% (from 4.47 m with q_1 = 1000 N/m to 1.08 m with q_5 = 3000 N/m).

Table 4: Maximum values of compressive strains and lateral displacement (buckle crown area) in the pre- and post-earthquake (EQ), with different friction coefficients and submerged weight and for OD/t = 20.

Parameter	ε_c (m/m)		y (m)	
μ_1	pre-EQ	post-EQ	pre-EQ	post-EQ
0.3	2.1519×10^{-3}	2.1532×10^{-3}	1.271	3.844
0.5	2.0663×10^{-3}	2.0651×10^{-3}	1.109	4.204
0.7	2.0037×10^{-3}	1.9984×10^{-3}	0.986	3.887
0.9	1.9597×10^{-3}	1.9484×10^{-3}	0.887	3.238
μ_2	pre-EQ	post-EQ	pre-EQ	post-EQ
0.1	1.7993×10^{-3}	1.9429×10^{-3}	2.606	4.375
0.3	2.0663×10^{-3}	2.0651×10^{-3}	1.109	4.204
0.5	9.9153×10^{-4}	2.1727×10^{-3}	0.117	3.725
0.7	9.9148×10^{-4}	2.1344×10^{-3}	0.029	3.251
μ_1-μ_2	pre-EQ	post-EQ	pre-EQ	post-EQ
0.3-0.1	1.8685×10^{-3}	1.7196×10^{-3}	3.019	4.318
0.5-0.3	2.0663×10^{-3}	2.0651×10^{-3}	1.109	4.204
0.7-0.5	9.9223×10^{-4}	2.1135×10^{-3}	0.106	3.552
0.9-0.7	9.9217×10^{-4}	1.9620×10^{-3}	0.023	2.775
q	pre-EQ	post-EQ	pre-EQ	post-EQ
1000	1.7267×10^{-3}	1.4012×10^{-3}	3.075	4.468
1500	2.0663×10^{-3}	2.0651×10^{-3}	1.109	4.204
2000	1.1412×10^{-3}	2.2359×10^{-3}	0.053	3.787
2500	1.2710×10^{-3}	2.4366×10^{-3}	0.012	2.900
3000	2.0532×10^{-3}	2.5021×10^{-3}	0.009	1.079

The highest jump in buckle amplitude is registered with small values of μ_2, as shown in the displacement time history in Figure 10b (from 2.6 m to 4.4 m). The most significant contribution in terms of reducing lateral displacement is obtained with the increase of both seabed and sleeper friction coefficients, and the submerged weight q, as discussed in previous studies [52–54]. These situations could be achieved with a roughened coating with enhanced textures [53] and a thicker coating or a more substantial surcharge on the pipeline laid on the seabed [52], respectively. This aspect allows to use higher operating temperatures and reduces the probability of lateral buckling during an earthquake. However, using high values of pipe-seabed-sleeper friction coefficient or submerged weight could have a significant impact on compressive strains built-up along the pipeline, as they can reach a peak value much higher than the yield point of the material, especially in the buckle crown of the pipeline. Nevertheless, high values of seabed-pipe friction coefficient (μ_1 = 0.9) could have positive effects on limiting the compressive strain along the pipeline away from the midpoint.

6 CONCLUSIONS

The response of HP/HT pipelines to the combined effects of seismic and thermal loadings have been assessed. In particular, flexural, thermal and thermal-seismic responses of pipelines with

OD/t from 10 to 50 were studied using FEA. The most significant contributions and findings of the current work are:

- Local wrinkles emerge in the compressive face of the pipeline at bending moments which correspond to development of yield surfaces in the wall thickness prior to reaching ultimate moment capacity of the pipeline. Failure occurs at moments slightly larger than the full plastic moment M_P and the ultimate moment capacity of the pipeline decreases with the corresponding increase in wall thickness (Stage I).
- Critical strains at Stage I are closer to the low safety class in DNV (2013) with the increase in OD/t, due to the higher risk of local collapse in thinner pipes ($OD/t > 30$). The calculated Stage I strains are within the proposed strain ranges of low safety class pipelines recommended in DNV (2013) at $OD/t < 30$.
- All the studied pipelines experienced compressive strains much lower than those corresponding to the ultimate moment capacity (Stage I) and those of DNV safety classes. Safety factors were calculated by comparing the buckle curvature and the normalised curvature at Stage I of the flexural response. It was understood that pipelines with $OD/t > 40$ are most vulnerable to failure due to local buckling under combined thermal-seismic actions.
- Significant contribution in reducing lateral displacement in pipelines was obtained by increasing both seabed and sleeper friction coefficients, and the submerged weight (i.e. enhancing surface roughness and changing surcharge material density). The combined variation of friction coefficients and submerged weight could improve the strain distribution along the pipeline, reducing the earthquake detrimental effects.

Future studies are recommended to investigate the interaction response of pipelines considering full-scale or scaled-down laboratory tests, more realistic pipe-soil interaction models, the surrounding seawater, and more sophisticated loss and recovery models.

REFERENCES

[1] Melissianos VE, Vamvatsikos D, Gantes CJ. Performance-based assessment of protection measures for buried pipes at strike-slip fault crossings. Soil Dynamics and Earthquake Engineering 2017;101:1–11. https://doi.org/10.1016/j.soildyn.2017.07.004.

[2] Turner J. Stones field-Installing the world's deepest FPSO and gas pipeline. Offshore Technology| Oil and Gas News and Market Analysis 2019.

[3] Karampour H, Alrsai M, Khalilpasha H, Albermani F. Experimental and Numerical Assessment on Failure Pressure of Textured Pipelines. Journal of Offshore Mechanics and Arctic Engineering 2022;144. https://doi.org/10.1115/1.4052475.

[4] Cunha DJS, Ferraz C, Netto TA, Diniz JC, Rosa DGG, Freire JLF. Hydrostatic Collapse Tests of Full-Scale Pipeline Specimens With Thickness Metal Loss. Volume 2: Pipeline Safety Management Systems; Project Management, Design, Construction, and Environmental Issues; Strain Based Design; Risk and Reliability; Northern, Offshore, and Production Pipelines, American Society of Mechanical Engineers; 2020. https://doi.org/10.1115/IPC2020-9562.

[5] Alrsai M, Karampour H, Hall W, Lindon AK, Albermani F. Carbon fibre buckle arrestors for offshore pipelines. Applied Ocean Research 2021;111:102633. https://doi.org/10.1016/j.apor.2021.102633.
[6] Stephan P, Love C, Albermani F, Karampour H. Experimental study on confined buckle propagation. Advanced Steel Construction 2016;12:44–54.
[7] Karampour H, Albermani F, Gross J. On lateral and upheaval buckling of subsea pipelines. Eng Struct 2013;52:317–30. https://doi.org/10.1016/j.engstruct.2013.02.037.
[8] Karampour H, Albermani F, Veidt M. Buckle interaction in deep subsea pipelines. Thin-Walled Structures 2013;72:113–20. https://doi.org/10.1016/j.tws.2013.07.003.
[9] Wang Z, Tang Y, van der Heijden GHM. Analytical study of lateral thermal buckling for subsea pipelines with sleeper. Thin-Walled Structures 2018;122:17–29. https://doi.org/10.1016/j.tws.2017.09.030.
[10] Choi HS. Free spanning analysis of offshore pipelines. Ocean Engineering 2001;28:1325–38. https://doi.org/10.1016/S0029-8018(00)00071-8.
[11] Piran F, Karampour H, Woodfield P. Numerical Simulation of Cross-Flow Vortex-Induced Vibration of Hexagonal Cylinders with Face and Corner Orientations at Low Reynolds Number. J Marine Science and Engineering 2020; 8(6), 387. http://dx.doi.org/10.3390/jmse8060387
[12] Karampour H. Effect of proximity of imperfections on buckle interaction in deep subsea pipelines. Marine Structures 2018;59:444–57. https://doi.org/10.1016/j.marstruc.2018.02.011.
[13] Binazir A, Karampour H, Sadowski AJ, Gilbert BP. Pure bending of pipe-in-pipe systems. Thin-Walled Structures 2019;145:106381. https://doi.org/10.1016/j.tws.2019.106381.
[14] Binazir A, Karampour H, Gilbert BP, Guan H. Bending Capacity of Pipe-in-Pipe Systems Subjected to External Pressure. ACMSM25, Singapore: Springer; 2020, p. 657–66. https://doi.org/10.1007/978-981-13-7603-0_64.
[15] Chen WW, Shih B, Chen Y-C, Hung J-H, Hwang HH. Seismic response of natural gas and water pipelines in the Ji-Ji earthquake. Soil Dynamics and Earthquake Engineering 2002;22:1209–14. https://doi.org/10.1016/S0267-7261(02)00149-5.
[16] Sakurai A, Takahashi T. Dynamic stresses of underground pipelines during earthquakes. Proceedings of the Fourth World Conference on Earthquake Engineering (Vol. 81), 1969.
[17] Housner GW, Jenningst PC. The San Fernando California earthquake. Earthq Eng Struct Dyn 1972;1:5–31.
[18] Hall JF, Holmes WT, Somers P. Northridge earthquake of January 17, 1994: reconnaissance report (Vol. 11). 1995.
[19] EQE International. The January 17, 1995 Kobe earthquake : an EQE summary report. San Francisco, USA: EQE International; 1995.
[20] O'Rourke M. Wave Propagation Damage to Continuous Pipe. TCLEE 2009, Reston, VA: American Society of Civil Engineers; 2009, p. 1–9. https://doi.org/10.1061/41050(357)76.
[21] Esposito S, Giovinazzi S, Elefante L, Iervolino I. Performance of the L'Aquila (central Italy) gas distribution network in the 2009 (Mw 6.3) earthquake. Bulletin of Earthquake Engineering 2013;11:2447–66. https://doi.org/10.1007/s10518-013-9478-8.
[22] Mori S, Chiba K, Koike T. Seismic performance analysis of the transmission gas pipeline in the 2011 great East Japan Earthquake. 15th World Conference on Earthquake Engineering (15WCEE), 2012, p. 24–8.

[23] O'Rourke MJ, Liu X. Response of buried pipelines subject to earthquake effects. Buffalo, NY: MCEER; 1999.
[24] Shi P. Seismic wave propagation effects on buried segmented pipelines. Soil Dynamics and Earthquake Engineering 2015;72:89–98. https://doi.org/10.1016/j.soildyn.2015.02.006.
[25] Takada S, Tanabe K. Three-Dimensional Seismic Response Analysis of Buried Continuous or Jointed Pipelines. J Press Vessel Technol 1987;109:80–7. https://doi.org/10.1115/1.3264859.
[26] Isoyama R, Ishida E, Yune K, Shirozu T. Seismic damage estimation procedure for water supply pipelines. 12th World Conference on Earthquake Engineering (Vol. 18), Auckland, New Zealand: 2000, p. 63–8.
[27] Jeon S-S, O'Rourke TD. Northridge Earthquake Effects on Pipelines and Residential Buildings. Bulletin of the Seismological Society of America 2005;95:294–318. https://doi.org/10.1785/0120040020.
[28] Han Z, Ma D, Hou B, Wang W. Seismic Resilience Enhancement of Urban Water Distribution System Using Restoration Priority of Pipeline Damages. Sustainability 2020;12:914. https://doi.org/10.3390/su12030914.
[29] American Lifelines Alliance (ALA). Seismic fragility formulations for water systems, Part I: Guideline 2001.
[30] Bi K, Hao H, Li C, Li H. Stochastic seismic response analysis of buried onshore and offshore pipelines. Soil Dynamics and Earthquake Engineering 2017;94:60–5. https://doi.org/10.1016/j.soildyn.2017.01.005.
[31] Uckan E, Akbas B, Shen J, Rou W, Paolacci F, O'Rourke M. A simplified analysis model for determining the seismic response of buried steel pipes at strike-slip fault crossings. Soil Dynamics and Earthquake Engineering 2015;75:55–65. https://doi.org/10.1016/j.soildyn.2015.03.001.
[32] Vazouras P, Dakoulas P, Karamanos SA. Pipe–soil interaction and pipeline performance under strike–slip fault movements. Soil Dynamics and Earthquake Engineering 2015;72:48–65. https://doi.org/10.1016/j.soildyn.2015.01.014.
[33] Mina D, Forcellini D, Karampour H. Analytical fragility curves for assessment of the seismic vulnerability of HP/HT unburied subsea pipelines. Soil Dynamics and Earthquake Engineering 2020;137:106308. https://doi.org/10.1016/j.soildyn.2020.106308.
[34] Forcellini D, Mina D, Karampour H. The Role of Soil Structure Interaction in the Fragility Assessment of HP/HT Unburied Subsea Pipelines. J Mar Sci Eng 2022;10:110. https://doi.org/10.3390/jmse10010110.
[35] DNV. Submarine pipeline systems 2007.
[36] DNV. DNVGL-RP-D101, Structural analysis of piping systems 2017.
[37] ABAQUS. Analysis user's guide 2020.
[38] Gresnigt AM, Karamanos SA. Local buckling strength and deformation capacity of pipes. The Nineteenth International Offshore and Polar Engineering Conference, Osaka, Japan: OnePetro; 2009.
[39] ABS. Guide for Building and Classing Subsea Pipelines Systems 2008.
[40] Kyriakides S, Ok A, Corona E. Localization and propagation of curvature under pure bending in steel tubes with Lüders bands. Int J Solids Struct 2008;45:3074–87. https://doi.org/10.1016/j.ijsolstr.2008.01.013.
[41] Hobbs RE. In-Service Buckling of Heated Pipelines. J Transp Eng 1984;110:175–89. https://doi.org/10.1061/(ASCE)0733-947X(1984)110:2(175).

[42] Li C, Hao H, Li H, Bi K. Theoretical modeling and numerical simulation of seismic motions at seafloor. Soil Dynamics and Earthquake Engineering 2015;77:220–5. https://doi.org/10.1016/j.soildyn.2015.05.016.
[43] Pan H, Li H-N, Li C, Tian L. Probabilistic seismic responses and failure analyses of free-spanning subsea pipelines under offshore spatial earthquake motions. Thin-Walled Structures 2022;179:109566. https://doi.org/10.1016/j.tws.2022.109566.
[44] Boore DM, Smith CE. Analysis of earthquake recordings obtained from the Seafloor Earthquake Measurement System (SEMS) instruments deployed off the coast of southern California. Bulletin of the Seismological Society of America 1999;89:260–74. https://doi.org/10.1785/BSSA0890010260.
[45] Li C, Hao H, Li H, Bi K, Chen B. Modeling and Simulation of Spatially Correlated Ground Motions at Multiple Onshore and Offshore Sites. Journal of Earthquake Engineering 2017;21:359–83. https://doi.org/10.1080/13632469.2016.1172375.
[46] Pan H, Li H-N, Li C. Seismic behaviors of free-spanning submarine pipelines subjected to multi-support earthquake motions within offshore sites. Ocean Engineering 2021;237:109606. https://doi.org/10.1016/j.oceaneng.2021.109606.
[47] Li C, Li H-N, Hao H, Bi K, Chen B. Seismic fragility analyses of sea-crossing cable-stayed bridges subjected to multi-support ground motions on offshore sites. Eng Struct 2018;165:441–56. https://doi.org/10.1016/j.engstruct.2018.03.066.
[48] Kalliontzis C. Numerical simulation of submarine pipelines in dynamic contact with a moving seabed. Earthq Eng Struct Dyn 1998;27:465–86. https://doi.org/10.1002/(SICI)1096-9845(199805)27:5<465::AID-EQE737>3.0.CO;2-X.
[49] DNV. DNV-RP-C205, Environmental conditions and environmental loads 2010.
[50] Ranf RT, Eberhard MO, Berry MP. Pacific Earthquake Engineering Research Center (PEER) 2001.
[51] Arifin RB, Wan M. Yusof WMSB, Zhao P, Bai Y. Seismic Analysis for the Subsea Pipeline System. 29th International Conference on Ocean, Offshore and Arctic Engineering: Volume 5, Parts A and B, ASMEDC; 2010, p. 659–67. https://doi.org/10.1115/OMAE2010-20671.
[52] Seth D, Manna B, Shahu JT, Fazeres-Ferradosa T, Pinto FT, Rosa-Santos PJ. Buckling Mechanism of Offshore Pipelines: A State of the Art. J Mar Sci Eng 2021;9:1074. https://doi.org/10.3390/jmse9101074.
[53] de Leeuw LW, Diambra A, Dietz M, Milewski H, Mylonakis G, Kwon OS, et al. Using coating roughness to control pipe-soil friction and influence pipeline global buckling behaviour. 4th International Symposium on Frontiers in Offshore Geotechnics, 2020.
[54] Hong Z, Fu D, Liu W, Zhou Z, Yan Y, Yan S. Effect of Gain in Soil Friction on the Walking Rate of Subsea Pipelines. J Mar Sci Eng 2019;7:401. https://doi.org/10.3390/jmse7110401.
[55] Cimellaro GP, Reinhorn AM, Bruneau M. Seismic resilience of a hospital system. Structure and Infrastructure Engineering 2010;6:127–44. https://doi.org/10.1080/15732470802663847.
[56] Cimellaro GP, Reinhorn AM, Bruneau M. Quantification of seismic resilience. Proceedings of the 8th US National conference on Earthquake Engineering (Vol. 8, No. 1094), 2006, p. 1–10.